ingegneria sismica
International Journal of Earthquake Engineering
Anno XLIII - Num. 3 - 2026

ANSYS-based residual stress control method and its optimization design in the process of straightening and side-straightening of linear guideway of machine tool

Long Fu[1,2,3,*]

[1] Ningbo Intelligent Machine Tool Research Institute Co., Ltd. of China National Machinery Institute Group, Ningbo, Zhejiang, 315700, China
[2] School of Mechanical Engineering, University of Science and Technology Beijing, Beijing, 100083, China
[3] China Academy of Machinery Science and Technology Group Co., Ltd., Beijing, 100044, China

SUMMARY: *Residual stresses are generated in the process of straightening and side-straightening of machine tool linear guideway, which affects the accuracy and service life of the guideway. In this study, the residual stress control method and optimization design of machine tool linear guide rail in the process of straightening and side-straightening are developed. Combining ANSYS finite element analysis and digital image correlation method for stress measurement, NSGA-II algorithm is used to construct a multi-objective optimization model. The experimental results show that the error between the stress measurement based on digital image correlation method and the finite element simulation results is within ±10%, which verifies the accuracy of the calculation model. The optimized process parameters of straightening stroke of 2.417 mm and grinding depth of 27.14 μm reduce the transverse residual stress of the guideway from 100 MPa to less than 15 MPa, and at the same time achieve the optimal combination of straightness error of 0.109 mm and roughness error of 2.62 μm. The study proves the effectiveness of the proposed residual stress regulation method in the process of positive and lateral straightening of linear guideway of machine tool, which provides theoretical support for improving the machining accuracy and performance of the guideway.*

KEYWORDS: *Linear guideway; residual stress; ANSYS; finite element analysis; NSGA-II algorithm; positive straightening side straightening*

1 Introduction

High-end CNC machine tools not only play an important role in the aerospace, military and nuclear industries and other strategic areas of national security, but also in the medical, inertial confinement fusion, microelectronics, high-performance parts/components of the precision manufacturing and other major fields play a key role [1-3]. With the continuous improvement of the mechanical manufacturing industry on the performance requirements of CNC machine tools, the global machine tool industry are actively exploring and developing more and better new manufacturing equipment, high-precision, high-speed and high-reliability high-end CNC machine tools have become the global machine tool industry to pursue and develop the direction [4, 5].

*d202110326@xs.ustb.edu.cn
https://doi.org/10.65102/is20261154
Published: 10 June, 2026

Due to the nature of the work, structural characteristics and other reasons that determine the majority of the machine tool is made of cast iron casting, and the complexity of the structure of the machine tool, the wall thickness is not uniform, the size of the disparity is too large, so the machine tool in the end of the manufacturing process, there will be a large number of residual stresses inside the machine tool, especially thermal stresses, which will lead to machine tool rails, such as the internal organization of the machine tool is in a temporary equilibrium and the instability of the state [6-9]. In order to maintain the stable operation of the linear guideway of the machine tool, the straightness and accuracy of the guideway of the machine tool can be repaired by means of positive or side straightening to maintain the stable operation of the machine tool [10]. However, in the straightening process, with the change of working conditions, the extension of time, the continuous change of linear guide temperature, linear guide wear and other phenomena, the stress balance is destroyed, the residual stress will continue to release, the bed will be deformed, and the linear guide part happens to be the dimensional accuracy requirements are high, the stress is easy to deformation of the components, linear guide as long as the deformation occurs, it will bring about the machining accuracy of the walk directly [11-13]. And in the cutting, cold bending and other machining processes, guideway straightening in the disappearance of external forces, guideway localized by mechanical stress, local guideway deformation [14]. In addition, the machine tool guideway straightening process, due to operation irregularities, straightening unreasonable factors will cause the linear guideway stress changes or re-stress concentration, the guideway material and shape changes, affecting the distribution of stress, leaving a hidden danger to the future continued deformation [15-17]. Based on this, it is of great value to explore the method of regulating the residual stress in the correction of linear guideways of machine tools.

As a key component of machine tool precision movement, the machining accuracy and surface quality of the linear guideway directly affect the overall performance of the machine tool. In the manufacturing process of the guideway, straightening and side straightening is an important part of eliminating geometric errors, but it also introduces residual stresses, which affects the mechanical properties and service life of the guideway. At present, there is a relative lack of research on the distribution of residual stress and its regulation method in the process of linear guide positive straightening and side straightening, which makes it difficult to realize the precise control of residual stress. Based on the elastic-plasticity theory and finite element method, this study constructs the residual stress prediction model in the linear guide rail straightening and side straightening process. Through ANSYS finite element analysis software, combined with the digital image correlation method measurement technology, the residual stress distribution in the guide rail straightening and side-straightening process was studied in depth. A multi-objective optimization model considering straightness error and roughness error is further established, and the NSGA-II algorithm is used to solve the optimal process parameter combination. The accuracy of the model is verified by three-point bending experiments, and the residual stress distribution of the guideway before and after optimization is analyzed comparatively. The study not only theoretically elucidates the formation mechanism of residual stress in the process of linear guideway straightening and side-straightening, but also puts forward a practical method of residual stress control, which provides new ideas and technical means to improve the processing accuracy and performance of the guideway.

2 Methodology

2.1 ANSYS-based finite element analysis of linear guideway of machine tool

ANSYS [18] is a powerful co-simulation platform, which has the following advantages: it has the interface of all mainstream software CAD software, realizes the transfer of all data including parameters, and is one of the advanced CAE tools in modern product design.

The finite element method [19] is an effective numerical calculation method developed along with the use of electronic computers, also known as the finite element method. The analysis process of applying the finite element method to solve elastic-plastic problems mainly includes the steps of discretizing the structure, selecting the displacement model, analyzing the characteristics of the units, and solving the equations.

2.1.1 Discretization of structures

The finite element discretization method of structure combining refers to a finite set of elements instead of cell and cell structure, only through the nodes are connected to each other, cell boundary displacement is guaranteed to be consistent. Usually should increase the density of the mesh in the stress change is relatively large or prone to stress, strain concentration place discrete structure, the division of the size, type and number of cells should be based on the needs of the project to determine the description of the deformation pattern should be determined by the calculation of accuracy and capacity.

2.1.2 Displacement mode selection

The mechanical properties of the unit are the relationship between nodes and node displacements, so it is necessary to set up a system of linear equations for node displacements with unknown displacement functions, and the displacement function of a simple tetrahedral unit is set as a linear function:

$$u = \alpha_1 + \alpha_2 x + \alpha_3 y + \alpha_4 \tag{1}$$

$$v = \alpha_s + \alpha_6 x + \alpha_\gamma y + \alpha_8 \tag{2}$$

$$w = \alpha_9 + \alpha_{10} x + \alpha_{11} y + \alpha_{12} \tag{3}$$

where: u, v, w is the displacement function of the tetrahedral cell, $\alpha_1, \alpha_2, ..., \alpha_{12}$ are the required coefficients.

Based on the displacements and coordinates of the nodes and thus the required coefficients, the shape function of the unit displacements is then introduced simplified as:

$$u = N_i u_i + N_j u_j + N_m u_m + N_p u_p \tag{4}$$

$$v = N_i v_i + N_j u_j + N_m v_m + N_p v_p \tag{5}$$

$$w = N_i w_i + N_j w_j + N_m w_m + N_p w_p \tag{6}$$

where $N_i = (a_i + b_i x + c_i y + d_i) / 6V$.

$N_j = (a_j + b_j x + c_j y + d_j)/6V$.

u_i, v_i, w_i are the node coordinates.

N_i, N_j, N_m, N_p are unit displacement shape functions.

$6V = \begin{vmatrix} 1 x_j & y_j & z_j \\ 1 x_m & y_m & z_m \\ 1 x_p & y_p & z_m \\ 1 x_p & y_p & z_p \end{vmatrix}$, V is the volume of the tetrahedral cell.

The coefficients $a_i = \begin{vmatrix} x_j & y_j & z_j \\ x_m & y_m & z_m \\ x_p & y_p & z_m \\ x_p & y_p & z_j \\ 1 & y_m & z_m \\ 1 & y_p & z_p \end{vmatrix} (i, j, m, p)$.

The coefficients $c_i = -\begin{vmatrix} x_j 1 z_j \\ x_m 1 z_m \\ x_p 1 z_p \end{vmatrix} (i, j, m, p)$.

Coefficients $d_i = -\begin{vmatrix} x_j y_j z_j \\ x_m y_m z_m \\ x_p y_p z_p \end{vmatrix} (i, j, m, p)$.

Its matrix form is shown in Eq:

$$f = N\delta^e \tag{7}$$

where f is the displacement function matrix, $f = [uwv]^T$.

N is the shape function lifting matrix.

δ^e is the unit node displacement column matrix.

2.1.3 Unit characterization

(1) Establishment of unit strain matrix:

$$\varepsilon = [\partial] \cdot f = [\partial] N \delta^e = B\delta^e \tag{8}$$

where $[\partial]$ is the geometric equation operator of elastodynamics.

ε is the strain matrix of the cell, $\varepsilon^e = [\varepsilon_x \varepsilon_y \varepsilon_s \gamma_{xy} \gamma_{yz} \gamma_{sx}]^T$.

B is a geometric constant matrix, $B = [B_i - B_j B_m - B_p]^T$.

δ^e is the unit node displacement matrix.

(2) Establishment of unit stress matrix:

$$\sigma = DB\delta^e = S\delta^e \tag{9}$$

where σ is the stress matrix of the unit cell, $\sigma = [\sigma_x \sigma_y \sigma_s \tau_{xy} \tau_{ys} \tau_{sx}]^T$.

D is the elasticity matrix in elastic mechanics.

S is the stress matrix of the cell, $S = [S_i - S_j S_m - S_p]^T$.

$$S_i = \frac{E(1-\mu)}{6(1+\mu)(1-2\mu)V} \begin{bmatrix} b_i & \Delta_1 c_i & \Delta_1 d_i \\ \Delta_1 b_i & c_i & \Delta_1 d_i \\ \Delta_1 b_i & \Delta_1 c_i & d_i \\ \Delta_2 c_i & \Delta_2 b_i & 0 \\ 0 & \Delta_2 d_i & \Delta_2 c_i \\ \Delta_2 d_i & 0 & \Delta_2 b_i \end{bmatrix} (i, j, m, p) \tag{10}$$

$$\Delta_1 = \frac{\mu}{1-\mu}, \Delta_2 = \frac{1-2\mu}{2(1-\mu)} \tag{11}$$

(3) Establishment of unit stiffness matrix:

$$K^e = \int_1 B^r DBdV \tag{12}$$

where: B is the geometric matrix. D is the elasticity matrix. After substituting the geometric and elastic matrices, it is obtained:

$$K^e = \begin{bmatrix} K_{ii} & -K_{ij} & K_{im} & -K_{ip} \\ -K_{ji} & K_{jj} & -K_{jm} & K_{jp} \\ K_{mi} & -K_{mj} & K_{mm} & -K_{mp} \\ -K_{pi} & K_{pj} & -K_{pm} & K_{pp} \end{bmatrix} \tag{13}$$

$$K_{\gamma s} = \frac{E(1-\mu)}{36(1+\mu)(1-\mu)V} \cdot \begin{bmatrix} b_\gamma b_s + \Delta_z(c_\gamma c_s + d_\gamma d_s) & \Delta_1 b_\gamma c_s + \Delta_z c_s b_s & \Delta_1 b_\gamma d_s + \Delta_z d_\gamma b_s \\ \Delta_1 c_\gamma b_s + \Delta_z b_\gamma c_s & c_\gamma c_s + \Delta_z(b_\gamma b_s + d_\gamma d_s) & \Delta_1 c_\gamma d_s + \Delta_z d_\gamma c_s \\ \Delta_1 d_\gamma b_s + \Delta_z b_\gamma d_s & \Delta_1 d_\gamma c_s + \Delta_z d_\gamma c_s & d_\gamma d_s + \Delta_z(b_\gamma b_s + c_\gamma c_s) \end{bmatrix} \quad (y, s = i, j, m, p) \tag{14}$$

(4) assembled into an overall stiffness equation:

$$\sum \Omega^e = \Omega \tag{15}$$

The node displacement δ is integrated as:

$$\delta = \sum \delta^e \tag{16}$$

Node Loading P Integrated:

$$P = \sum P^e \tag{17}$$

Equation for overall stiffness:

$$K \cdot \delta = P \tag{18}$$

Based on the listed system of equilibrium equations, the stresses, strains, etc. of any cell and unknown nodes can be found.

(5) Introduce boundary conditions such that the system of equations has a unique solution for a given load, i.e., the structural displacements can be determined uniquely, avoiding the possibility of the structure occurring as a whole.

(6) Solve for unknown degrees of freedom and solve for unit strains and stresses. This step solves the matrix equations and obtains the results of the equivalent quantities of nodal displacements, strains and stresses.

(7) Interpretation of the results, the processed results were visualized and the results were interpreted and analyzed using a graphical display. When performing structural design and analysis, it is necessary to determine the location of maximum displacements and stresses in the structure.

2.2 Measurement of linear guide straightening residual stress distribution

Based on the digital image correlation method, the principle of pressure straightening, the stress-strain model of the material and the elastic-plastic bending theory, this paper proposes a new method for measuring the residual stress in the process of linear guideway positive straightening and side straightening, and designs and develops the corresponding characterization algorithm program.

This section will be built around the linear guide rail straightening stress measurement experimental system to realize the measurement of the residual stress distribution in the linear guide rail straightening side straightening process. Three-point bending experiment to simulate the linear guide rail straightening side straightening process, the use of self-constructed digital image acquisition system on the linear guide rail in the three-point bending test bending deformation image acquisition, and then the acquisition of continuous deformation of the scattering image into the improved two-dimensional digital image correlation method of strain and stress calculation software to analyze and process, to get the guide rail in the bending process of the full-field displacement and strain, the strain results are calculated based on the strain results of the guide rail surface residual stress distribution. Based on the strain results, the stress and residual stress distribution on the rail surface are calculated. Finally, the use of ANSYS finite element simulation software on the bending process of linear guideway finite element simulation simulation analysis, and the results of the simulation and the use of this paper to build the experimental measurement system for the experimental measurement results of the relevant comparative analysis.

2.2.1 Three-point bending experimental setup

The equipment used in this three-point bending experiment is DNS100 universal material testing machine, whose maximum test force is 100KN, and the moving speed of the beam ranges from 0.005 to 500mm/min, with a resolution higher than 0.001mm, which fully meets the requirements of this three-point bending experiment. In this paper, the three-point bending experiment is in the universal material testing machine, to realize the loading bending and unloading springback deformation of the linear guide.

2.2.2 Stress measurement system based on digital image correlation method

This paper independently built a stress measurement experiment system based on digital image correlation method, the system mainly includes digital image acquisition system and digital image correlation method of strain stress calculation software system, Figure 1 shows the digital image correlation method of residual stress calculation software processing flow. In order to get a stable and clear scattering image of the deformation area on the surface of the linear guide rail during the bending process, a simple and stable digital image acquisition system for the bending process of the linear guide rail was designed and built, which mainly consists of two sub-systems: hardware and software. Hardware subsystem mainly includes industrial cameras, external auxiliary light source and acquisition computer and other parts.

Image acquisition software subsystem for the industrial camera comes with the acquisition software, by setting the relevant parameters of the camera on the software (including exposure time, image resolution, number of sampling frames, etc.), you can realize the bending process of the linear rail surface scattering images of the clear display and preservation.

The strain and stress calculation software is based on two-dimensional digital image correlation method designed and written by the strain and stress calculation software. Two-dimensional digital image correlation method strain calculation software can be used to calculate the strain field of the deformation zone on the surface of the linear guide rail by matching the irregular scattered images sprayed on the surface of the curved guide rail. On the basis of its design to add the function of stress calculation, through the two-dimensional digital image correlation method of strain calculation software output strain calculation results are processed and analyzed, so as to obtain the results of stress calculation.

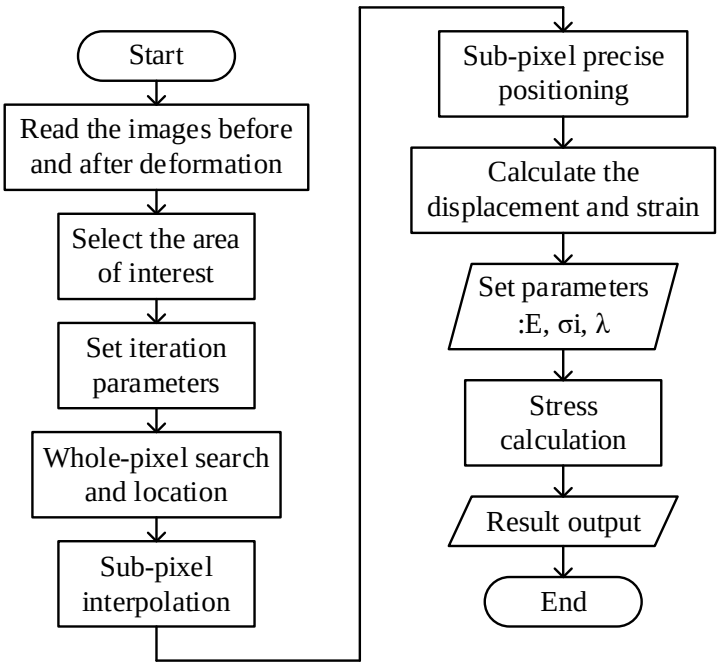

Figure 1: Residual stress calculation software processing process

2.3 Optimization of Residual Stress Regulation in Linear Guide Positive and Side Straightening Processes

In order to get the best comprehensive performance of positive and side straightening of linear guideway, this section establishes the optimization model of linear guideway straightening and grinding process. According to the processing requirements of the linear guide, the optimization

objectives are small geometric error, high surface accuracy and good mechanical properties. The optimized parameters are straightening process parameters and grinding process parameters. In order to accurately obtain the required optimization model, this paper combines the macro-geometry error and meso-geometry error into straightness error, and the micro-geometry error into roughness error.

2.3.1 Optimization objectives

There are 2 optimization objectives, including:

(1) Straightness error (STE)

The straightness error of the guideway in the straightening and grinding process can be regarded as the superposition of the straightness error change of the guideway in the straightening and side straightening process and the straightness error change in the grinding process. The straightness error of the guideway after the straightening process can be expressed as follows:

$$\delta_r = \delta_0 + \frac{2}{3}\frac{\sigma_s}{EH}\frac{l^2}{(C_\Sigma - C_0)^2}\left[5-(3+C_\Sigma - C_0)\sqrt{3-2(C_\Sigma - C_0)}\right] - S \tag{19}$$

The straightness error of the guideway after the grinding process can be expressed according to the surface geometry error model of the workpiece after grinding as follows:

$$\begin{cases} w_{mn}^i = \min\{w_{mn}^{i-1}, z_{mn}\} \\ \delta_g = \max(w_{mn}^i) - \min(w_{mn}^i) \end{cases} \tag{20}$$

The straightness error (STE) of the guideway after the straightening and grinding process is therefore:

$$STE = \delta_r + \delta_g \tag{21}$$

(2) Roughness error (RE)

Roughness error is also an important guideline in the guideway machining process. In the grinding process, the grinding wheel removes the material on the surface of the guideway, so the grinding process has a great influence on the roughness error of the guideway surface. The roughness error of the guideway can be expressed by considering only the grinding process parameters:

$$RE = \begin{cases} 0.4587 \times T_a^{0.30}, 0 < T_a \le 0.254 \\ 0.7866 \times T_a^{0.72}, 0.254 < T_a \le 2.540 \end{cases} \tag{22}$$

where T_a denotes the average chip thickness for grinding. The T_a is related to the grinding process and can be expressed as follows:

$$T_a = 12.5 \times 10^3 \times \frac{d_g^{16/27} \times a_p^{19/27}}{d_e^{8/27}} \times \left(1+\frac{doc}{L_d}\right) \times L_d^{16/27} \times \left(\frac{v_w}{v_s}\right)^{16/27} \tag{23}$$

where d_g denotes the grinding wheel grit size, a_p denotes the grinding depth, d_e denotes

the grinding wheel diameter, doc denotes the grinding wheel dressing depth, L_d denotes the grinding wheel dressing feed, v_w denotes the workpiece feed, and v_s denotes the grinding wheel speed.

2.3.2 Decision-making variables

There are 2 decision variables, including:

(1) Straightening stroke (STS)

Straightening stroke is the distance between the initial position of the lower pressure point and the termination position of the guide rail during straightening, which has an effect on both the elastic and plastic deformation amount of the positive and lateral straightening process, and ultimately affects the straightness error of the straightening process.

(2) Grinding depth (PA)

Grinding depth refers to the depth of the grinding wheel cutting the surface of the guideway when grinding, which has a great influence on the grinding temperature of the grinding process, the deformation of the guideway surface and the roughness error of the guideway, so the grinding speed will affect the straightness error and roughness error of the guideway.

2.3.3 Optimization constraints

After determining the optimization objective and optimization parameters, it is also necessary to determine the constraints of the optimization model. The constraints in this paper are as follows:

(1) Thermal damage constraints

The grinding process generates a large amount of heat, which is mainly concentrated in the grinding region of the workpiece and will reduce the productivity of grinding. The thermal damage of grinding is directly related to the specific grinding energy, and the specific grinding energy U can be expressed as:

$$\begin{aligned} U = & 13.8 + \frac{9.64\times10^{-4} v_s}{a_p v_w} \\ & + \left(6.9\times10^{-3} + \frac{2102.4\times v_w}{D_e v_s}\right)\left(A_0 + \frac{K_u v_s L_w a_w}{v_w D_e^{0.5} a_p^{0.5}}\right)\frac{v_s D_e^{0.5}}{v_w a_p^{0.5}} \end{aligned} \tag{24}$$

where A_0 denotes the initial wear plane area percentage and K_u denotes the wear constant.

The critical specific grinding energy U^* corresponding to the onset of grinding thermal damage can be expressed as:

$$U^* = 6.2 + 1.76\frac{D_e^{1/4}}{a_p^{3/4} v_w^{1/3}} \tag{25}$$

In order to ensure that no burns occur during the grinding process, the actual specific grinding energy should not exceed the critical specific grinding energy. Thus the thermal damage constraint can be expressed as:

$$U \le U^* \tag{26}$$

(2) Constraints on grinding wheel wear parameters

The grinding wheel wear parameter WWP is directly related to the grinding conditions. The grinding wheel wear parameter for single point grinding can be expressed as:

$$WWP = \frac{K_a a_p d_g^{5/38} R_c^{27/19}}{D_e^{(1.2/VOL-43/304)} VOL^{0.38}} \times \frac{(1+Doc/L)L^{27/19}(v_s/v_w)^{3/19} v_w}{(1+2Doc/3L)} \tag{27}$$

where VOL is the bond rate of the wheel and K_a is a constant dependent on the coolant and grit type.

The grinding wheel wear parameter constraint is usually expressed using the ratio of WWP and WRP, i.e., the following equation:

$$WRP / WWP \geq G \tag{28}$$

Where G denotes the grinding ratio and WRP denotes the material removal parameter of the workpiece, WRP is defined as the following equation:

$$WRP = 94.4 \frac{\left(1+\frac{2Doc}{3L}\right) L^{11/19} \left(\frac{v_w}{v_s}\right)^{3/19} v_s}{D_e^{43/304} VOL^{0.47} d_g^{5/38} R_c^{27/19}} \tag{29}$$

where Doc denotes the grinding wheel dressing depth, D_e denotes the grinding wheel diameter, and R_e is the Rockwell hardness value.

(3) Machine Stiffness Constraints

In order to avoid excessive chatter in grinding, the grinding stiffness, grinding wheel wear stiffness and machine static stiffness should satisfy the following constraints:

$$\frac{1}{2K_c}\left(1+\frac{v_w}{v_s G}\right)+\frac{1}{K_s} \geq \frac{|R_{em}|}{K_m} \tag{30}$$

where K_m is the static stiffness of the machine and R_{em} is the dynamic characteristics of the machine.

(4) Surface roughness constraint

In rough grinding machining, the following constraints on surface roughness are required to obtain maximum productivity while maintaining the desired accuracy:

$$R_a \leq R_a^* \tag{31}$$

where R_a^* denotes the maximum acceptable roughness.

(5) Productivity constraints

In finish grinding, the following constraints on productivity are required to obtain the best surface accuracy while maintaining productivity:

$$WRP \leq WRP^* \tag{32}$$

where WRP^* denotes the maximum acceptable grinding productivity.

2.4 NGSA-II based multi-objective optimization solution

The NSGA-II algorithm [20] process is as follows:

(1) Randomly generate an initial population P_0 of size N, perform a fast non-dominated sort grading and congestion computation on the population P_0 and assign fitness values to each solution according to the fitness function, and obtain the first-generation offspring population Q_0 by operations such as selection, crossover and mutation.

(2) Combine the parent population P_0 with the offspring population Q_0 into a new mixed population with a population size of $2N$, and use an elite retention strategy to search through the mixed population to produce the next generation of parent population P_1.

(3) Then generate a new offspring population Q_1 by crossover and mutation in P_1.

(4) Repeat steps (2) and (3) until the maximum number of iterations is reached.

3 Results and analysis

3.1 Convergence analysis of linear guide deflection values

The finite element method, combined with elastic-plastic finite element analysis, is used to create a finite element model and set the parameters of the model. For guide rails with different deflections, the straightening stroke is calculated according to the straightening prediction model, and Ansys is used to simulate the loading of the guide rails and solve the data. The straightening test is carried out by the method of three-point reverse bending straightening, and the deflection value of the loading point is measured online by the displacement sensor mounted on the straightening machine. The diameter of 10mm, the length of 400, 500, 600mm circular guide rail each 1, the material for the No. 45 steel, divided into three experimental groups.

The circular guide rail were labeled as 1, 2, 3, according to the order of the 3 groups of guide rail initial deflection measurements, and substituting into the model of multiple straightening stroke, the corresponding straightening stroke is calculated, to be released to the stress after the measurement of the residual deflection of the guide rail. Then according to the residual deflection to continue to iterate the calculation, and again derive the straightening stroke, in the linear guideway to complete the corresponding straightening steps; repeat the above process until the residual deflection control in the straightness requirements.

After three groups of tests, the guide rail deflection value convergence test results shown in Table 1. In the test, straightening samples using the same material linear guide, for multiple straightening stroke model for straightening test. Analysis of the results of the three comparison groups shows that the residual deflection value tends to converge in the process of multiple straightening, i.e., the straightness error is gradually reduced, indicating the correctness of the travel prediction model. In the case of the same length and the same cross-section parameters, the main factor affecting the number of straightening times and the straightening effect is the initial deflection of the straightening object.

Table 1: Guide deflection test results

Rail span(mm)	Parameter	Straightening number			
		1	2	3	4
400	Initial deflection	1.759	0.153	-0.127	-
	Cross section	3.411	2.035	-1.966	-
	Residual deflection	0.143	-0.173	0.101	-
500	Initial deflection	1.457	0.397	-0.143	-
	Cross section	7.585	6.377	-5.327	-
	Residual deflection	0.413	-0.185	-0.108	-
600	Initial deflection	3.691	1.082	-0.283	0.268
	Cross section	9.993	7.551	-7.912	7.367
	Residual deflection	0.405	-0.372	0.238	0.177

3.2 Finite Element Analog Simulation of Linear Guide Material

To ensure that the experiment is closer to the finite element simulation state, the linear guide material is annealed. The plate was heated to 600°C, held for 3h, and cooled with the furnace to eliminate the initial residual stress of the plate. The residual stresses before and after straightening were detected by the blind hole method. A small hole with a depth of 1.8mm is drilled on the surface of the part, and when the hole is punched layer by layer, the residual stress will be redistributed along the direction of plate thickness, and the strain values of each layer are read for calculation.

A multi-group experimental testing method is used, where each group of experiments is tested five times and the average value is taken to ensure the accuracy of the experiments. The stress measurement device based on the digital image correlation method above is used to realize the stress test of the plate layer by layer. By extracting the displacement trajectory of the neutral layer position of the plate thickness and comparing it with the trajectory of the curvature integral model, the comparison results of the trajectory of the straightening process are shown in Fig. 2, which shows that the curvature integral calculation and the finite element simulation are almost overlapped, which verifies the high precision and accuracy of the calculation of the curvature integral trajectory and in which the solid line area indicates the occurrence of plastic deformation, and the dotted line occurs the elastic resumption and elastic deformation.

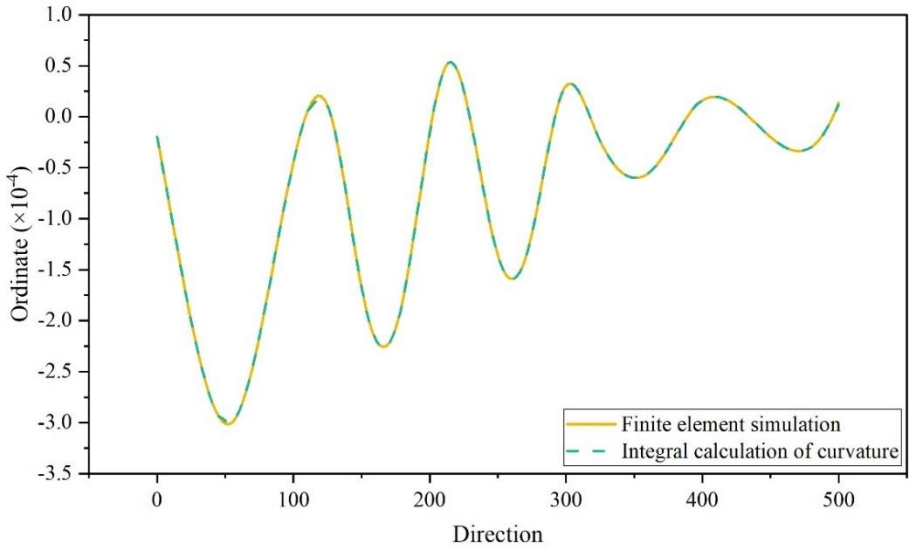

Figure 2: The straightening process trajectory compares results

The curvature of the straightening process obtained from the curvature integral is given by the following equation:

$$L_i = \frac{T_i}{2} R\sin\theta_i - R\sin\theta_{i+1} \tag{33}$$

L_i is the straightening roll spacing (m), R is the radius of the straightening roll (m), and θ_i straightens the indirect contact angle of each zone (°).

When the plate is subjected to the bending force of the working roll of the straightening machine exceeding the yield stress, the bending moment $M_i(x)$ is able to cause plastic deformation of the plate. At this time, the strain ε_w and stress σ_w are calculated as shown in Eq:

$$\begin{aligned} &\varepsilon_w = k_w z(-H/2 \le z \le H/2) \\ &\sigma_w = \begin{cases} E\varepsilon_w(-H_t/2 \le z \le H_t/2) \\ \sigma_t(-H_t/2 \le z \le H/2; H_t/2 \le z \le H/2) \end{cases} \end{aligned} \tag{34}$$

When the force is unloaded, the plate springs back layer by layer under the action of the plate's elastic recuperative energy, with the elastic deformation region fully sprung back and the plastic deformation region partially sprung back. Considering the continuity of the material, the self-equilibrium of the cross-section, the compression that occurs in the side layers, and the stretching that occurs in the heart, the final state of compressive and tensile stresses is formed. Calculation of the magnitude of residual strain ε_c and stress σ_c is shown in Eq:

$$\begin{aligned} &\varepsilon_c = (\varepsilon_w - \varepsilon_t) - k_c z(-H/2 \le z \le H/2) \\ &\sigma_c = E\varepsilon_c \end{aligned} \tag{35}$$

The residual stress after straightening is calculated, and the average value of finite element simulation and 5 experiments are compared, and the results of the comparison between experimental and calculated residual stress after straightening are shown in Figure 3. It can be seen from the figure, after annealing treatment of the guide material, after straightening the plate thickness direction stress is folded state, and the calculated stress size and experimental trend is consistent with the difference is not large, the error is within ± 10%. The main reason is caused by the neutral layer offset and work hardening in the straightening process, but the stress trend region is consistent, verifying the accuracy of the calculation. Among them, the theoretical calculations and simulations assume zero stress state of the original plate, and the experiments, although annealing treatment, there still exists a small amount of residual stress, so the simulation and calculation of the middle of the plate has a small change in residual stress, while the experiments show a large deviation. Other reasons for the error in the values are: the vibration error when punching holes in the blind hole method, and the theoretical calculation of the process material using ideal material properties, which is related to the actual material package Singer effect and so on.

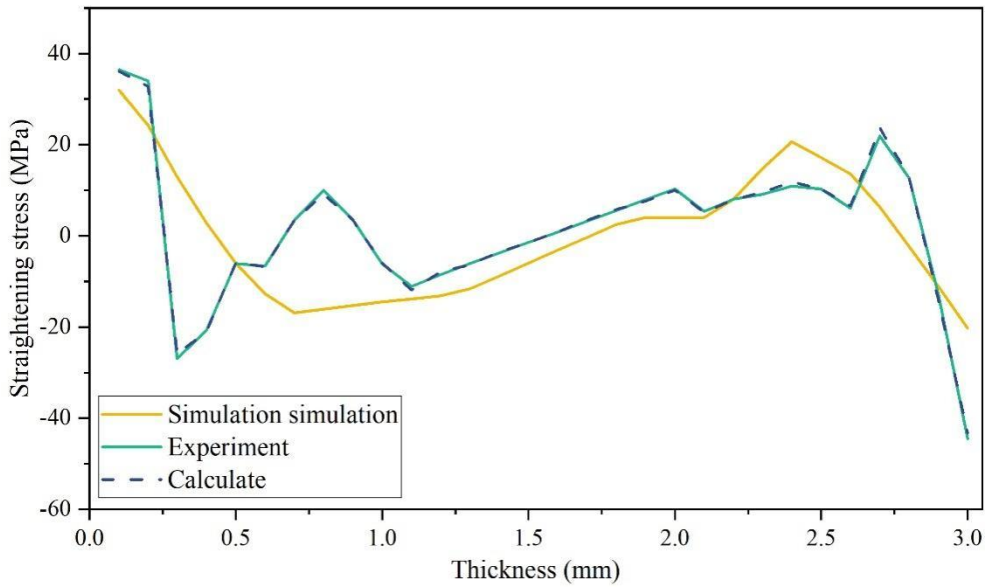

Figure 3: The results of the residual stress experiment and calculation were compared

3.3 Pareto optimal solution sets

The objective function and constraints of process parameter optimization are nonlinear and have both equal and unequal constraints, which belongs to the constrained nonlinear planning problem. Through the multi-objective optimization function based on NSGA-II, the parameters are set as follows: the population size is 200, the maximum number of evolutionary generations is 500, the optimal front-end individual coefficient is 0.2, and the deviation of the fitness function is 0.0002. In order to fully ensure the algorithm's global search ability, the initial population should be representative, and the initial population is obtained by choosing a consistent randomized way. The spatial distribution of the obtained Pareto optimal solution set is shown in Figure 4.

From the figure, it can be seen that these solution elements are uniformly distributed in the whole space, and in line with the definition of multi-objective optimization: the relationship between the objectives is constrained by each other, and there is no one solution that is completely dominant in two objectives. Compared with single-objective optimization, all 25 solution elements in the figure can be used as a set of optimization solutions, thus bringing more choices to the designers. The general trend of the two objective functions shows that the larger the surrogate value of straightness error (STE), the smaller the roughness error (RE). The main reason for this phenomenon is. The objective of the optimization model is the sum of straightness error and roughness error. Therefore, this paper adopts a compromise solution, i.e., the optimization objective is: STE = 0.109 mm, RE = 2.62 μm. The optimal solution corresponding to the optimal objective is the straightening stroke STS = 2.417 mm and the grinding depth PA = 27.14 μm.

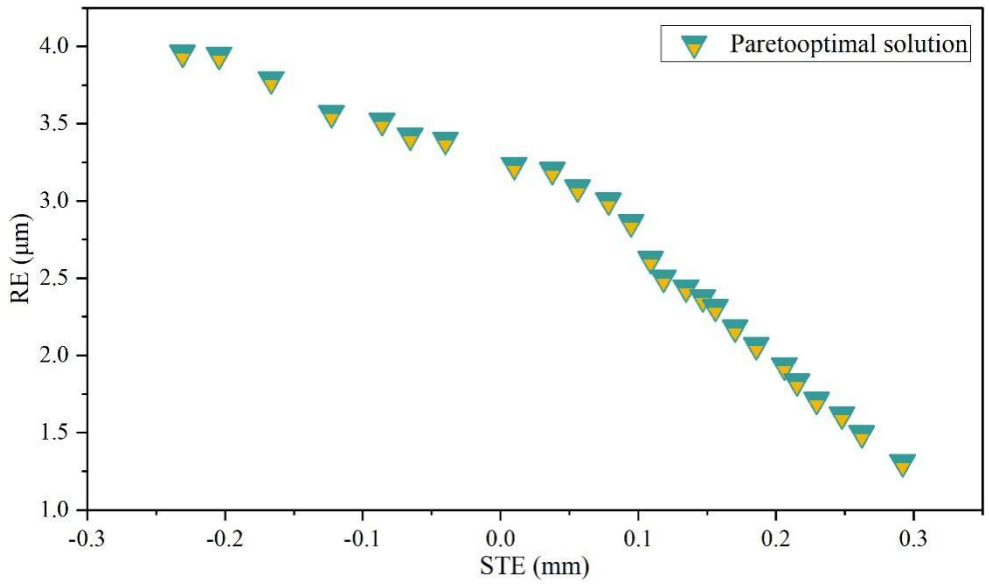

Figure 4: The optimal solution set space distribution of Pareto

3.4 Residual stress distribution of guideway before and after optimization

In order to verify the correctness of the optimization model, 20 machine tool samples in the online database of a machine tool factory are randomly extracted, and information such as the material and online setting of the underpressure of these varieties are extracted, and the optimization process in this paper is used for the optimization of process parameters, and the distribution of residual stresses in the process of positive and side straightening of the machine tool's linear guideway before and after the optimization is compared. Through the optimization, it is found that the selected optimization samples they have better consistency.

Figure 5 shows the lateral residual stress distribution before and after optimization. It can be seen that when the width of the guideway is 0, the residual stress distribution of the guideway before and after optimization is the highest. This is because when the width is close to 0, the deformation of the material in the transverse direction is strongly constrained, resulting in the stress cannot be effectively released through plastic deformation, so that the residual stress reaches the maximum value in the local area. Before optimization, the lateral residual stress distribution of the guideway is within 100 MPa, while after optimization it can be controlled within 15 MPa, which shows that the residual stress has been well reduced. This proves the effectiveness of the method of regulating the residual stress distribution by optimizing the parameters of the straightening and side-straightening process in this paper.

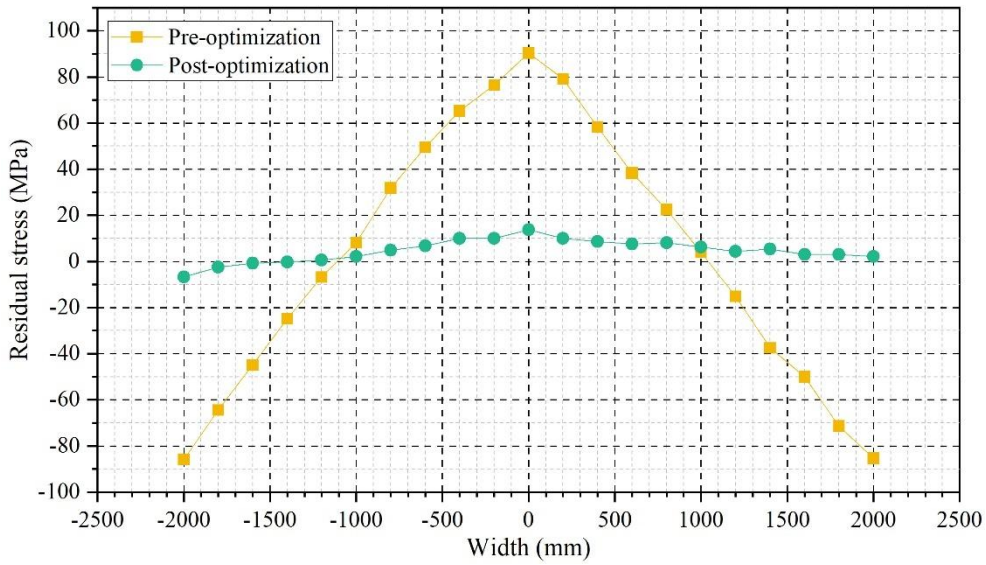

Figure 5: The distribution of lateral residual stress was optimized

4 Conclusion

The residual stress regulation method and optimization design in the process of straightening and side-straightening of linear guideway of machine tool proposed in this study have achieved remarkable results. Through the finite element analysis and experimental comparison verification, the error between the calculated and experimental values of residual stress after straightening is controlled within ±10%, which proves the accuracy of the model. The convergence test of the deflection value of the guideway shows that for the three specifications of 400mm, 500mm and 600mm, the final residual deflection reaches 0.101mm, 0.108mm and 0.177mm, respectively, which indicates that the established model of multiple straightening strokes can effectively improve the straightness of the guideway. The multi-objective optimization based on NSGA-II algorithm obtains 25 groups of Pareto optimal solutions, among which the best compromise scheme determines the optimal process parameter combinations of straightening stroke of 2.417mm and grinding depth of 27.14μm. Comparison before and after optimization shows that the transverse residual stress of the guideway is reduced from 100MPa to less than 15MPa, which is 85% less, and the synergistic optimization of straightness error and roughness error is realized at the same time. The results show that the guideway residual stress distribution can be significantly improved and the machining accuracy and performance can be enhanced by reasonably regulating the positive and lateral straightening process parameters. The method proposed in this study provides important theoretical support and practical process guidance for the precision machining of machine tool linear guideways.

About the Authors

Long Fu is a doctoral student majoring in Mechanical Engineering at the School of Mechanical Engineering, Beijing University of Science and Technology, Beijing, China. His research interests include advanced manufacturing, ANSYS simulation, and neural networks.

Weimin Long, Researcher, doctoral supervisor, chief scientist of China General Institute of Machinery Group, winner of the 2nd National Science and Technology Innovation Competition, innovative talent of the 3rd National "Ten Thousand Talents Program", winner of the 4th National Outstanding Engineer, expert of special allowance of the State Council, winner of

Henan Science and Technology Outstanding Contribution Award, winner of Ningbo "Outstanding Talent", chief expert of Ningbo Intelligent Machine Tool Research Institute Co., Ltd. of China General Institute of Machinery Group. Director of the South Center of the Chinese Academy of Mechanical Sciences.

Dong Xiang, As the (sub) project leader, responsible for 14 national projects and 4 enterprise projects; As the main researcher, I have undertaken 8 national research projects. Obtained 33 authorized invention patents; Published 21 SCI indexed papers as the first and second authors, and participated in the compilation of 5 textbooks and monographs. Received 2 first prizes and 3 second prizes at the provincial, ministerial, and association levels, and was honored as an advanced technology worker in the machinery industry.

References

[1] Bomba, G., & Gierlak, P. (2020). Assessment of geometric accuracy of a 5-axis CNC machine in the context of machining aircraft transmission housings. Univ. J. Mech. Eng, 8, 257-263.

[2] Pathak, C., & Kumari, S. (2025). CNC machines in production and manufacturing of medical devices. Artificial Intelligence in Biomedical and Modern Healthcare Informatics, 393-401.

[3] Peterka, J., Kuruc, M., Kolesnyk, V., Dehtiarov, I., Moravcikova, J., Vopat, T., ... & Simna, V. (2023). Selected aspects of precision machining on CNC machine tools. Machines, 11(10), 946.

[4] Xu, X. (2017). Machine Tool 4.0 for the new era of manufacturing. The International Journal of Advanced Manufacturing Technology, 92, 1893-1900.

[5] Yao, K. C., Chen, D. C., Pan, C. H., & Lin, C. L. (2024). The development trends of computer numerical control (CNC) machine tool technology. Mathematics, 12(13), 1923.

[6] Soori, M., & Arezoo, B. (2022). A review in machining-induced residual stress. Journal of New Technology and Materials, 12(1), 64-83.

[7] Sunny, S., Mathews, R., Gleason, G., Malik, A., & Halley, J. (2021). Effect of metal additive manufacturing residual stress on post-process machining-induced stress and distortion. International Journal of Mechanical Sciences, 202, 106534.

[8] Wan, N., He, Q., Jiang, Y., Zhou, H., & Fu, B. (2023). Numerical and experimental investigation of the influence of the machining parameters on residual stress distribution of internal thread cold extrusion. CIRP Journal of Manufacturing Science and Technology, 40, 142-154.

[9] Xiang, S., Deng, M., Li, H., Du, Z., & Yang, J. (2019). Cross-rail deformation modeling, measurement and compensation for a gantry slideway grinding machine considering thermal effects. Measurement Science and Technology, 30(6), 065007.

[10] Liu, M., Xia, Y., Lu, H., Zhang, Y., Zang, Y., & Li, L. (2021, March). A Straightening Control System for the Linear Guide Rail. In 2021 IEEE 5th Advanced Information Technology, Electronic and Automation Control Conference (IAEAC) (pp. 1169-1173).

IEEE.

[11] Carvalho, M. F., Rodrigues, L. D., & Lins, E. F. (2021). Analysis of residual stresses in rails during the straightening process. Journal of the Brazilian Society of Mechanical Sciences and Engineering, 43(1), 1.

[12] Zang, Y., Zhang, Y., Yu, L., Lu, H., Liu, Z., & Wang, Y. (2025). The effect of residual stress on the multi-step multi-point straightening with the three-dimensionally deformed linear guideway. Proceedings of the Institution of Mechanical Engineers, Part C: Journal of Mechanical Engineering Science, 239(3), 789-806.

[13] Zhang, Y., Lu, H., Ling, H., Lian, Y., & Ma, M. (2018). Analytical model of a multi-step straightening process for linear guideways considering neutral axis deviation. Symmetry, 10(8), 316.

[14] Ling, H., Yang, C., Feng, S., & Lu, H. (2020). Predictive model of grinding residual stress for linear guideway considering straightening history. International Journal of Mechanical Sciences, 176, 105536.

[15] Fang, Y., Ling, H., & Lu, H. (2019, April). Study on reverse bending characteristics in straightening process considering the stress superposition. In IOP Conference Series: Earth and Environmental Science (Vol. 252, No. 2, p. 022116). IOP Publishing.

[16] Song, Y. (2019). Load-deflection model for T-section rail press straightening process under lateral loads. Cluster Computing, 22, 2955-2961.

[17] Shelest, A. E., Yusupov, V. S., Karelin, R. D., & Perkas, M. M. (2022). Geometric and deformation parameters of elastoplastic alternating bending of a strip during processing on a roller straightening machine. Russian Metallurgy (Metally), 2022(5), 546-551.

[18] Kadir Kaya,Mehmet Dorduncu & Erdogan Madenci. (2025). Variable horizon ordinary state-based peridynamic analysis in ANSYS framework. Mechanics of Advanced Materials and Structures,32(9),2079-2095.

[19] Tianlong He,Philippe Karamian Surville & Daniel Choï. (2025). Phantom Domain Finite Element Method: A novel approach for heterogeneous materials. Applications in Engineering Science,22,100218-100218.

[20] Han Yang,Ninghao Liu,Maomeng Li,Mengjie Gu & Qiang Gao. (2025). Design and optimization of heat pipe-assisted liquid cooling structure for power battery thermal management based on NSGA-II and entropy Weight-TOPSIS method. Applied Thermal Engineering,272,126416-126416.